

The Ultrasound Needle Pulse

Kevin J. Parker, *Fellow, IEEE*, Shujie Chen, *Student Member, IEEE*, and Miguel A. Alonso

Abstract—Recent theoretical developments have defined the conditions for forming a broadband beam that is narrow in axial extent but extended in range. The formulation is based on the classical angular spectrum decomposition and the requirement for arranging all spatial and temporal frequencies such that all components have constant phase propagation between planes. Analytic formulations are given for a 1-D source and a 2-D axisymmetric source, and comparisons are made against conventional focused Gaussian beams under similar conditions relevant to medical imaging systems.

Index Terms—Medical beamforming and beam steering, medical imaging, system and device design, underwater ultrasound.

I. INTRODUCTION

THE study of beampatterns and their use in imaging systems has a long history in optics and acoustics. Imaging systems may transmit spherically spreading waves from small elements, as in synthetic aperture systems, or plane (unfocused) waves as in high frame rate systems, or focused beams as in conventional phased array ultrasound systems [1]–[4].

In addition, the topic of propagation invariant (or limited diffraction) fields has received increasing attention since the characterization of Bessel beams in optics [5]. The class of “localized waves” includes Mathieu beams [6], X-beams [7], Airy beams [8], [9], and related monochromatic and broadband solutions [10].

Recently, we formulated a new class of propagation invariant fields based on the principle of a wideband source excitation configured through the angular spectrum, such that all components propagate with equal phase in the forward propagating direction [11]. Analytic solutions are obtained for a 1-D source, then for an axial symmetric source, and for a pulsed version of the field. The free-space solution has some remarkable properties, including vanishing group velocity and a convergence of all energy to a narrow central line as a spatial and temporal crescendo, hence the appellation “needle pulse.” Dynamic visualizations are given online in links found in [11]; these demonstrate the convergence of waveform to the crescendo and subsequent divergence. In the needle pulse, there is no focusing in the conventional sense,

and the excitation of a source that is composed of 1-D or 2-D array elements can be realized by sampling bounded input waveforms that are expressed in an analytical form.

In this paper, we provide an introduction to the characteristics of the needle pulse fields and their implementation in ultrasound linear array transducers. The needle pulse field is compared against more conventional Gaussian beams, which have been studied in optics and acoustics [12]–[16].

II. THEORY

The mathematical conditions for the isophase propagation have been recently described by Parker and Alonso [11], and the solutions were developed within the framework of the angular spectrum [17]–[19]. The isophase condition was also recently studied by [20]. Here, we recapitulate the key solutions to the scalar wave equation.

We first examine the simplest case, where the source is distributed along a line in the x -direction, and z is the direction of forward propagation. This starting point has numerous applications, since many practical applications in acoustics, medical ultrasound, and radar use 1-D arrays. Furthermore, 2-D arrays can be excited using separable, orthogonal, 1-D functions. For 1-D sources, the isophase condition reduces to constant k_z over all source frequencies ω and wavenumbers k_x

$$k_z = \left(\frac{\omega}{c}\right)^2 - k_x^2 = k_L^2. \quad (1)$$

Let us choose a lowest, or base frequency ω_L , defined as a plane wave in the z -direction, so

$$k_L^2 = \left(\frac{\omega_L}{c}\right)^2. \quad (2)$$

All higher frequencies $\omega \geq \omega_L$ of a broadband source can meet the isophase condition. In a dispersion-free medium such as a free space where $c(\omega) = c_0$

$$k_x^2 = \frac{1}{c_0^2}(\omega^2 - \omega_L^2). \quad (3)$$

This defines a hyperbola in the 2-D Fourier space of $[k_x, \omega]$.

The solution to the isophase angular spectrum integral is found to be given in the compact form

$$p(x, z, t) = \frac{c_0}{2} K_0 [k_L \sqrt{x^2 - c_0^2(t - iq)^2}] \exp(ik_L z) \quad (4)$$

where p is the complex pressure, c is the speed of sound, and t is time. Furthermore, $k_L = \omega_L/c$ and K_0 is a modified Bessel function of the second kind of order 0, and the branch cut of the square root is assumed at the negative real axis of its argument.

Manuscript received December 15, 2016; accepted April 6, 2017. Date of publication April 7, 2017; date of current version July 1, 2017. The work of K. J. Parker and S. Chen was supported by the Hajim School of Engineering and Applied Sciences, University of Rochester. The work of M. A. Alonso was supported by the National Science Foundation under Grant PHY-1507278. (Corresponding author: Kevin J. Parker.)

K. J. Parker and S. Chen are with the Department of Electrical and Computer Engineering, University of Rochester, Rochester, NY 14627 USA (e-mail: kevin.parker@rochester.edu; shujie.chen@rochester.edu).

M. A. Alonso is with The Institute of Optics, University of Rochester, Rochester, NY 14627 USA (e-mail: miguel.alonso@rochester.edu).

Digital Object Identifier 10.1109/TUFFC.2017.2692562

Note that $t = 0$ does not correspond to the initial time but to the time at which the field is most concentrated spatially; in theory, the excitation must exist for all negative times. The parameter q determines the bandwidth of the spectrum used, and therefore how narrow the field becomes at $t = 0$. The parameter q can be understood as an imaginary offset to the time axis in (4), or as an exponential decay applied to either k_x or ω in (3).

To generate this field, the broadband source distribution at plane $z = 0$ is simply the real part of (4) with $z = 0$. For 1-D arrays in ultrasound applications, spatial samples of this would constitute the source excitation signals, typically voltages applied to the individual subwavelength elements of the 1-D array.

A. Solutions in Three Dimensions With Rotational Symmetry

Analogous results can be found for fields in three dimensions. For example, the following finite-power solution exists, which has rotational symmetry:

$$p(\rho, z, t) = c_0 \frac{\exp[-k_L \sqrt{\rho^2 - c_0^2(t - iq)^2}]}{k_L \sqrt{\rho^2 - c_0^2(t - iq)^2}} \exp(ik_L z) \quad (5)$$

where $\rho = (x^2 + y^2)^{1/2}$. These solutions have approximately spherical wavefronts, and they have a full width of approximately $2(c_0^2 t^2 + q^2)^{1/2}$, and the parameter q regulates how spatially localized these solutions are at $t = 0$.

B. Needle Pulses With Limited Energy

The issue of limits on energy and power is important in localized waves. For example, the ideal continuous Bessel beam [5] has an infinite number of rings, and therefore over an infinite source area would carry infinite power [21]. Limiting the energy of needle pulses is particularly easy to achieve with the 3-D pulses in (5), whose dependence in k_L is simply as a linear factor in the exponent and a global factor of k_L^{-1} . One can find closed-form finite-energy solutions simply by integrating in k_L the product of (5) with k_L and a weight function of k_L centered around a longitudinal wavenumber K_L and whose inverse Fourier transform can be found analytically

$$\begin{aligned} p_2(\rho, z, t) &= \int_{-\infty}^{\infty} k_L p(\rho, z, t) F(k_L - K_L) dk_L \\ &= p(\rho, z, t)|_{k_L=K_L} f(z + i\sqrt{\rho^2 - c_0^2(t - iq)^2}) \quad (6) \end{aligned}$$

where $F(k_z)$ is the Fourier transform of $f(z)$. That is, the finite-energy solution is just the product of the infinite-energy solution times an envelope analytic function of a complex argument. For example, using a Gaussian weight of width δ gives

$$\begin{aligned} p_2(\rho, z, t) &= \int_{-\infty}^{\infty} k_L p(\rho, z, t) \frac{1}{\sqrt{2\pi}\delta} \exp\left[-\frac{(k_L - K_L)^2}{2\delta^2}\right] dk_L \\ &= p(\rho, z, t)|_{k_L=K_L} \\ &\quad \times \exp\left[-\frac{\delta^2}{2}(z + i\sqrt{\rho^2 - c_0^2(t - iq)^2})^2\right]. \quad (7) \end{aligned}$$

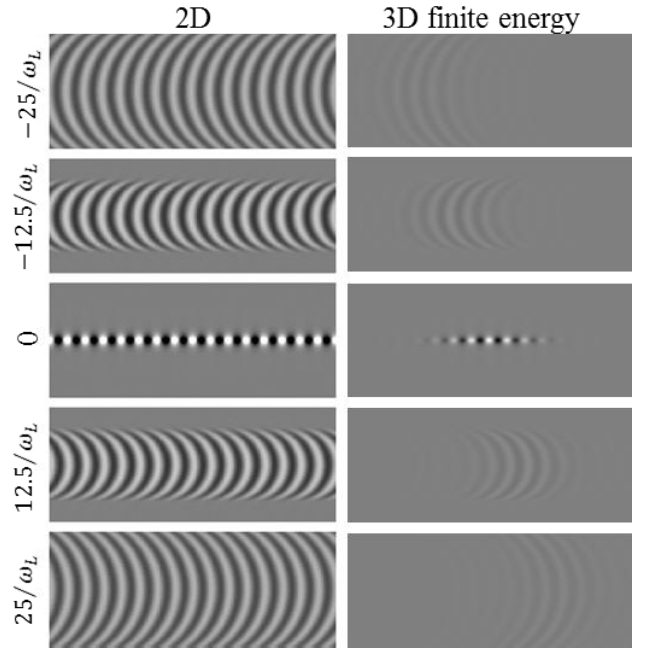


Fig. 1. Theoretical solutions for (left) 2-D solution (4) and (right) pulsed 3-D solution in (7), at five different times and with $\omega_L q = 1$. Left: $x \in [-20/k_L, 20/k_L]$ (vertical) and $z \in [0, 100/k_L]$ (horizontal). Right: $x \in [-20/K_L, 20/K_L]$ and $z \in [-50/K_L, 50/K_L]$.

The fields produced in the case of the 2-D solution (4) and for the pulsed axisymmetric 3-D solution (7) are shown in Fig. 1. In both cases, the longitudinal pressure wave appears as converging, then concentrating, and then diverging along the central axis.

III. METHODS

In both the 2-D and 3-D pulsed solutions, it is natural to assume the source plane is $z = 0$. However, there is no such restriction; in fact, the source plane can be identified in theory with any reasonable value of z . In the following examples, the excitation voltage waveform supplied to the acoustic array elements is given by the real part of (4), (5), or (7) with a negative value of z , assuming the peak spatial intensity (in the pulsed case) will appear near $z = 0$. Field II [22], [23] simulations were conducted to generate the acoustic pressure field of the needle pulse excitation. The 2-D needle pulse (7) with $z = -10$ mm, $q = 0.4$, and $s = 0.2$ was sampled at 100 MHz in time and used as the excitation signal of a 16 mm \times 16 mm 2-D linear array transducer. The transducer has an impulse response of a 6-MHz Gaussian-modulated sine with 70% bandwidth and a pitch of 0.125 mm, or $\lambda/2$ at 6 MHz. This was apodized using a Planck-taper window ($\varepsilon = 0.118$) in both dimensions to enforce a smooth transition to zero at the extreme edge elements. The speed of sound was set to 1500 m/s.

IV. RESULTS

The amplitude (left) and pressure waves (right) for the needle pulse are given in Fig. 2. Note that with the source excitation taken as $z = -10$ mm, the peak spatial amplitude

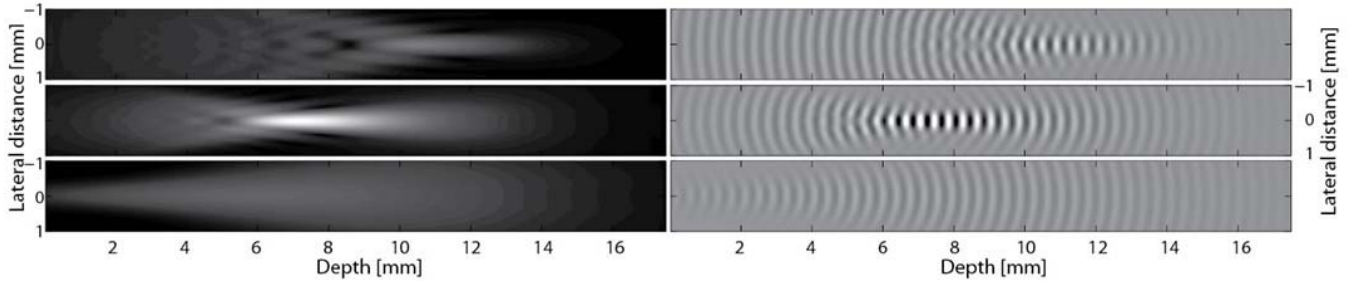


Fig. 2. Amplitude (left) and pressure waves (right) at three time instants (top to bottom, $t = -2, 0,$ and $2 \mu\text{s}$ from peak) resulting from a 2-D array with a center frequency of 6 MHz, 70% bandwidth, and 16-mm square. The source excitation waveform was the real part of (7) with the parameters: $q = 0.4$, $\omega_L = 2\pi \cdot 4$ MHz, and $z_{\text{source}} = -10$ mm. Note that the top-left amplitude has been multiplied by 1.25, so that it appears visible.

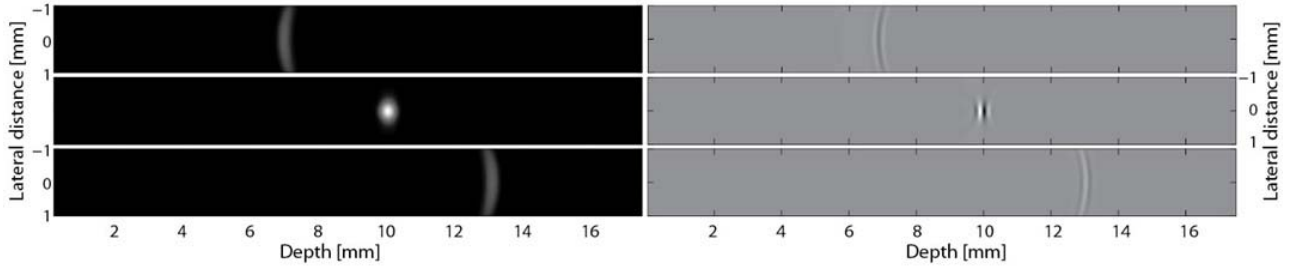


Fig. 3. Amplitude (left) and pressure waves (right) at three time instants (top to bottom, $t = -2, 0,$ and $2 \mu\text{s}$ from peak) resulting from a 2-D array with a center frequency of 6 MHz, 70% bandwidth, and 16-mm square. The source excitation is an impulse with spherical time delays set for a focus of 10 mm.

occurs near $z = 8$ mm in this instance. In comparison, the Gaussian focused pulse (Fig. 3) with focus set to 10 mm reaches a spatial peak near this depth.

V. DISCUSSION

Of particular interest is the comparison of the axisymmetric needle pulse versus a more traditional axisymmetric focused Gaussian broadband pulse using the same 2-D array. In theory, at the point of crescendo, the needle pulse beamwidth has a lateral beamwidth given by: $[\exp(-k_L(\rho^2 + c_0^2 q^2)^{1/2})]/(k_L(\rho^2 + c_0^2 q^2)^{1/2})$, and asymptotically (for larger ρ), this drops off as $[\exp(-k_L \rho)]/k_L \rho$, producing a high-resolution single lobe with no sidelobes.

In comparison, an ideal narrowband focused Gaussian will have a Gaussian beampattern, with comparatively faster asymptotic decay as a function of ρ , and with no sidelobes. However, in practice, this is never achieved, first because of the need to truncate the Gaussian [24], [25] producing unwanted sidelobes, and second because broadband pulses are preferred for imaging. The solution for a two-way (transmit/receive) beampattern from a broadband focused Gaussian pulse has been recently derived [26], and is given by

$$H_f^{bG}(\rho; B, \sigma_0) = \frac{\sqrt{\frac{\pi}{2}} f_0 \exp\left(-\frac{D^2 \rho^2}{2D^2 \sigma_0^2 + 2B^2 \rho^2}\right) \left[\operatorname{erf}\left(\frac{2\sqrt{2}}{B \sqrt{\frac{1}{\ln 2} \left(\frac{B^2 \rho^2}{D^2 \sigma_0^2} + 1\right)}}\right) + 1 \right]}{\sqrt{\frac{\rho^2}{\sigma_0^2} + \frac{D^2}{B^2}}} \quad (8)$$

where $D = 4\sqrt{\ln 2}$, $\operatorname{erf}(\cdot)$ is the error function, f_0 and σ_0 are the center frequency and focal beamwidth at center

frequency, respectively, and B is the system bandwidth expressed as a fraction. Fig. 4 shows four curves, theoretical versus Field II, for both needle pulse and pulsed Gaussian using the same 6 MHz array parameters for each case.

The broadband focused Gaussian was simulated in Field II [22], [23] using the same 2-D transducer array except that the apodization of the transducer was changed to a 2-D 6- σ Gaussian function, and the excitation signal became an impulse. The transducer was focused at 10 mm below its center along the axial direction.

The comparison demonstrates a close match between theory and Field II simulations near the central axis maximum. However, strictly limiting the active source to 16×16 mm causes additional truncation effects that deviate from the theoretical result. This is seen as sidelobes near the -20 - and -35 -dB levels in Fig. 4, where the effect of the limited support for the needle pulse at the source plane acts as an abrupt truncation of the ideal excitation function. This effect is related to the form of the solution of (4), (5), and (7) where the functions have local maxima near $r = ct$. So the excitation pulse for larger values of time requires larger values of r to represent that portion of the waveform. The examples in Fig. 4 correspond to low f -number. For the broadband Gaussian example, the f -number is $10/16 = 0.625$, which pertains to “close-up” applications. Larger f -numbers can be implemented, but the truncation effects (sidelobes) need to be reexamined in these applications.

VI. CONCLUSION

The ultrasound needle pulse is formed by arranging all the spatial and temporal frequencies within some practical bandwidth into waves that propagate with constant phase between the source plane and an arbitrary parallel plane.

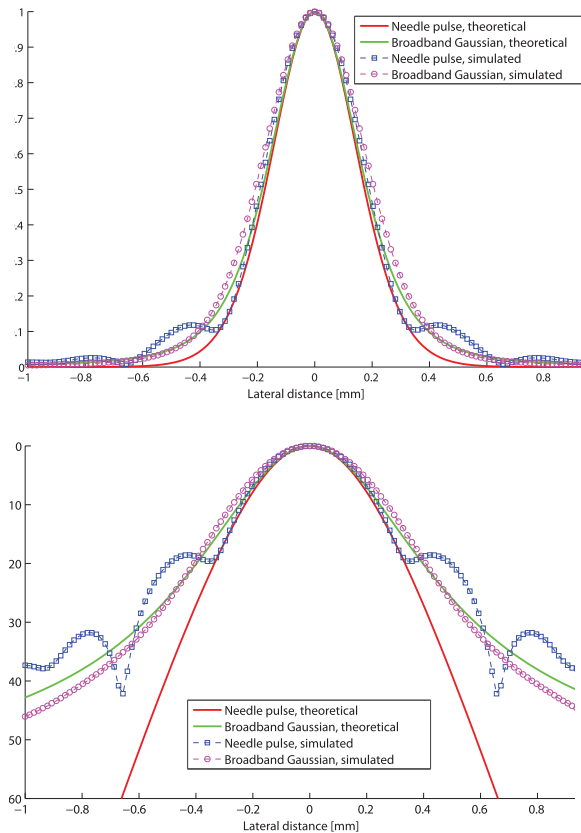


Fig. 4. Lateral envelope (amplitude) at temporal and spatial peak for the transmitted needle pulse and the conventional broadband focused pulse. Both cases set to produce a nominal $z = 10$ -mm spatial peak. Top: linear plots. Bottom: log scale. Theory assumes continuous apodization across an infinite source; simulation uses $r \leq 8$ -mm 2-D linear array.

The solutions yield converging stacks of pressure waves that form into a long axis peak and then diverge. At the point of maximum convergence, the lateral beamwidth is compact with no sidelobes. The needle pulse is sensitive to truncation of the excitation waveform supplied to the transducer elements, in time and space, and so the examples here are equivalent to a low f -number system: a diameter of 16 mm and a focal length, or z offset, of 10 mm. There are a number of possible applications in imaging, in radiation force techniques, and in nonlinear heating and cavitation studies, that could benefit from the unique properties of the needle pulse. These remain to be explored in the future research.

REFERENCES

- [1] K. K. Shung, *Diagnostic Ultrasound: Imaging and Blood Flow Measurements*, 2nd ed. Boca Raton, FL, USA: CRC Press, 2015, ch. 3.
- [2] K. E. Thomenius, "Evolution of ultrasound beamformers," in *Proc. IEEE Ultrason. Symp.*, vol. 2, Nov. 1996, pp. 1615–1622.
- [3] R. S. C. Cobbold, *Foundations of Biomedical Ultrasound*. New York, NY, USA: Oxford Univ. Press, 2007, ch. 8.
- [4] T. L. Szabo, *Diagnostic Ultrasound Imaging: Inside Out*. Burlington, MA, USA: Elsevier, 2004, ch. 10.
- [5] J. Durmin, "Exact solutions for nondiffracting beams. I. The scalar theory," *J. Opt. Soc. Amer. A, Opt. Image Sci.*, vol. 4, no. 4, pp. 651–654, 1987.
- [6] J. C. Gutiérrez-Vega, M. D. Iturbe-Castillo, and S. Chávez-Cerda, "Alternative formulation for invariant optical fields: Mathieu beams," *Opt. Lett.*, vol. 25, no. 20, pp. 1493–1495, 2000.

- [7] J.-Y. Lu and J. F. Greenleaf, "Nondiffracting X waves—exact solutions to free-space scalar wave equation and their finite aperture realizations," *IEEE Trans. Ultrason., Ferroelectr., Freq. Control*, vol. 39, no. 1, pp. 19–31, Jan. 1992.
- [8] M. V. Berry and N. L. Balazs, "Nonspreading wave packets," *Amer. J. Phys.*, vol. 47, no. 3, pp. 264–267, 1979.
- [9] G. A. Siviloglou and D. N. Christodoulides, "Accelerating finite energy Airy beams," *Opt. Lett.*, vol. 32, no. 8, pp. 979–981, 2007.
- [10] H. E. Hernández, M. Zamboni-Rached, and E. Recami, *Localized Waves*. Hoboken, NJ, USA: Wiley, 2008.
- [11] K. J. Parker and M. A. Alonso, "Longitudinal iso-phase condition and needle pulses," *Opt. Exp.*, vol. 24, no. 25, pp. 28669–28677, 2016.
- [12] D. Ding and X. Liu, "Approximate description for Bessel, Bessel–Gauss, and Gaussian beams with finite aperture," *J. Opt. Soc. Amer. A, Opt. Image Sci.*, vol. 16, no. 6, pp. 1286–1293, 1999.
- [13] D. Huang and M. A. Breazeale, "An ultrasonic Gaussian transducer and its diffraction field: Theory and practice," *IEEE Trans. Ultrason., Ferroelectr., Freq. Control*, vol. 53, no. 5, pp. 1018–1027, May 2006.
- [14] P. L. Marston, "Quasi-Gaussian beam analytical basis and comparison with an alternative approach (L)," *J. Acoust. Soc. Amer.*, vol. 130, no. 3, pp. 1091–1094, 2011.
- [15] G. Du and M. A. Breazeale, "The ultrasonic field of a Gaussian transducer," *J. Acoust. Soc. Amer.*, vol. 78, no. 6, pp. 2083–2086, 1985.
- [16] J.-Y. Lu, H. Zou, and J. F. Greenleaf, "Biomedical ultrasound beam forming," *Ultrasound Med. Biol.*, vol. 20, no. 5, pp. 403–428, 1994.
- [17] M. Born and E. Wolf, *Principles of Optics: Electromagnetic Theory of Propagation, Interference and Diffraction of Light*. New York, NY, USA: Pergamon Press, 1980, ch. 11, pp. 556–592.
- [18] J. W. Goodman, *Introduction to Fourier Optics*, 3rd ed. Englewood, CO, USA: Roberts & Co., 2005, ch. 3.
- [19] M. Born, *Principles of Optics: Electromagnetic Theory of Propagation, Interference and Diffraction of Light*. New York, NY, USA: Pergamon Press, 1980, ch. 11, p. 1.
- [20] H. E. Kondakci and A. F. Abouraddy, "Diffraction-free pulsed optical beams via space-time correlations," *Opt. Exp.*, vol. 24, no. 25, pp. 28659–28668, Dec. 2016.
- [21] D. McGloin and K. Dholakia, "Bessel beams: Diffraction in a new light," *Contemp. Phys.*, vol. 46, no. 1, pp. 15–28, 2005.
- [22] J. A. Jensen, "Deconvolution of ultrasound images," *Ultrason. Imag.*, vol. 14, no. 1, pp. 1–15, Jan. 1992.
- [23] J. A. Jensen, "Simulation of advanced ultrasound systems using field II," in *Proc. 2nd IEEE Int. Symp. Biomed. Imag., Nano Macro*, vol. 1, Apr. 2004, pp. 636–639.
- [24] K. J. Parker, "Correspondence: Apodization and windowing functions," *IEEE Trans. Ultrason., Ferroelectr., Freq. Control*, vol. 60, no. 6, pp. 1263–1271, Jun. 2013.
- [25] K. J. Parker, "Correspondence—Apodization and windowing eigenfunctions," *IEEE Trans. Ultrason., Ferroelectr., Freq. Control*, vol. 61, no. 9, pp. 1575–1579, Sep. 2014.
- [26] S. Chen and K. J. Parker, "Enhanced resolution pulse-echo imaging with stabilized pulses," *J. Med. Imag.*, vol. 3, no. 2, pp. 027003-1–027003-13, Jun. 2016.



Kevin J. Parker (S'79–M'81–SM'87–F'95) received the master's and Ph.D. degrees from Massachusetts Institute of Technology, Cambridge, MA, USA.

He has served as a Department Chair with the University of Rochester, Rochester, NY, USA, the Director of the Rochester Center for Biomedical Ultrasound, University of Rochester, and the Dean of the Hajim School Engineering and Applied Sciences, University of Rochester. He is currently the William F. May Professor of Engineering with the University of Rochester. He is an inventor/pioneer in a number of enterprises, including the field of sonoelastography and the international conference series in that area, and the Blue Noise Mask. He is a founder of VirtualScopics, Inc., Rochester, NY. He has published 200 journal articles and numerous book chapters. He holds 25 U.S. patents and 13 international patents that have been licensed to 25 companies. His current research interests include image processing and medical imaging.

Dr. Parker is a fellow of the AIUM, ASA, and AIMBE. He was a recipient of the Eastman Medal, the AIUM Joseph Holmes Pioneer Award for Contributions to Medical Ultrasound, the Eastman Kodak Outstanding Innovation Award, and the Ultrasound in Medicine and Biology World Federation Prize.



Shujie Chen (S'14) received the B.S. degree in communications engineering from the Nanjing University of Posts and Telecommunications, Nanjing, China, in 2007, and the M.S. degree in electrical engineering from the University of Rochester, Rochester, NY, USA, in 2013, where he is currently pursuing the Ph.D. degree with the Department of Electrical and Computer Engineering.

He was a Signal Processing Intern with MathWorks, Natick, MA, USA, in 2016. His current research interests include ultrasound imaging and image processing.



Miguel A. Alonso received the Engineering degree in physics from Universidad Autónoma Metropolitana, Mexico City, Mexico, in 1990, and the Ph.D. degree in optics from the University of Rochester, Rochester, NY, USA, in 1996.

He is currently a Professor with The Institute of Optics, University of Rochester. He is also a member of the Center for Freeform Optics and the Center for Coherence and Quantum Optics, University of Rochester.

Dr. Alonso is a fellow of the Optical Society of America. He was an Associate Editor and a Deputy Editor of the journal *Optics Express* from 2002 to 2013. He is an Associate Editor of the journal *Optica*.